Journal of Power Sources 195 (2010) 6831–6838

Contents lists available at ScienceDirect

Journal of Power Sources

journal homepage: www.elsevier.com/locate/jpowsour

Electrochemically active silver molybdenum oxyfluoride perovskite: Synthesis and in situ electrochemical characterization

W. Tong[a,b,*], W.-S. Yoon[c,1], G.G. Amatucci[a,b]

[a] Energy Storage Research Group, Department of Materials Science and Engineering, Rutgers, The State University of New Jersey, Piscataway, NJ 08854, USA
[b] Department of Biomedical Engineering, Rutgers, The State University of New Jersey, Piscataway, NJ 08854, USA
[c] Brookhaven National Laboratory, Upton, NY 11973, USA

ARTICLE INFO

Article history:
Received 15 March 2010
Received in revised form 13 April 2010
Accepted 14 April 2010
Available online 21 April 2010

Keywords:
Silver molybdenum oxyfluoride perovskite
positive electrode
Primary lithium battery
In situ XAS
Raman
XRD

ABSTRACT

An electrochemical characterization of a silver molybdenum oxyfluoride perovskite positive electrode for Li batteries was investigated as a function of synthesis condition, stoichiometry and effect of Mo and Ag derived second phases. A detailed in situ electrochemical study by XAS, Raman, and XRD was performed, revealing a 3 electron silver displacement or conversion reaction at >3 V and a 2 electron reduction of Mo^{6+} to Mo^{4+} in the region <3 V.

1. Introduction

Research has been focused on obtaining cathode materials with a higher energy density for rechargeable and primary Li batteries. A potential application for these higher energy cathode materials will be in implantable biomedical devices (cardiac pacemaker, drug pump, neurostimulator and cardioverter defibrillator [1]). Materials and manufacturing costs are not limiting when compared to the advantages of a battery made for this specific application (high-energy density, voltage >3 V, reliability and predictability, etc.) [2,3]. Presently, the commonly used Li battery system is Li/CF_1 for relatively low drain rate applications and $Li/Ag_2V_4O_{11}$ and its oxyfluoride derivatives ($Ag_4V_2O_6F_2$) for higher rate applications in biomedical community [4,5]. However, there is an ever present need for improved materials with the advent of new implantable applications such as congestive heart failure and cochlear implants.

Recently, we have identified a new compound, silver molybdenum oxyfluoride (SMOF) cryolite-like perovskite, of the proposed formula $Ag_3{}^{1+}Mo^{6+}(O_3F_3)$ via mechanochemical synthesis through the use of silver fluorides and molybdenum oxides [6,7]. Preliminary electrochemical characterization showed that the electroactivity of SMOF perovskite was enabled even without the use of conductive carbon matrix, suggesting the as-fabricated SMOF perovskite has appreciable mixed conductivity.

We have shown that SMOF perovskites fabricated using AgF precursors exhibited an interesting electrochemical property as an alternative high-energy density primary electrode material. A high volumetric energy density of ~2570 Wh L^{-1} was achieved at the 1st plateau (>3 V) for the SMOF material. In situ XRD indicated that a silver based conversion/displacement reaction took place in the SMOF perovskite at the plateaus >3 V. The main thrust of this communication is to shed light on the lithiation mechanism that ensues throughout the 5 electron reduction. This is brought forth with the use of in situ XRD, Raman, and XAS. In addition, the structure/property relationship of SMOF perovskite is examined in greater detail specifically related to the effect of phase homogeneity on the electrochemical properties.

2. Experimental

2.1. High-energy milling (HEM)

Silver molybdenum oxyfluoride (SMOF) perovskites were fabricated by the high-energy milling of 1 g stoichiometric precursors, which were prepared by manually mixing commercially available

* Corresponding author at: Energy Storage Research Group, Department of Materials Science and Engineering, Rutgers, The State University of New Jersey, Piscataway, NJ 08854, USA. Tel.: +1 732 932 6850; fax: +1 732 932 6855.
E-mail address: weitong@eden.rutgers.edu (W. Tong).
[1] Present address: School of Advanced Materials Engineering, Kookmin University, 861-1 Jeongneung-dong, Seongbuk-gu, Seoul 136-702, Republic of Korea.

0378-7753/$ – see front matter © 2010 Elsevier B.V. All rights reserved.
doi:10.1016/j.jpowsour.2010.04.043

MoO_3 (Alfa Aesar, 99.95%) and AgF (Aldrich, 99%) with an agate mortar and pestle. Both the high-energy milling cell and media were made of hardened steel. The high-energy milling cell was sealed and reopened in a He-filled glove box to minimize the moisture and/or air contamination. The milling was performed in a Spex 8000 Certiprep mixer/mill for the designated time. Unless otherwise noted, SMOF perovskites fabricated by high-energy milling for 45 min were utilized for general characterization.

2.2. Physical characterization: XRD

XRD patterns were collected on a Scintag X2 diffractometer with Cu Kα radiation by scanning each sample in the range of 15–80° at a rate of 0.6° min^{-1}. The materials to be analyzed were placed on a glass slide and covered with Kapton film sealed with a layer of vacuum grease around the perimeter in the glove box to reduce moisture and/or oxygen contamination. In situ XRD was performed in a house-made in situ XRD cell utilizing a Be window. The electrochemical cell was cycled at a constant current of 3 mA g^{-1} (2.37 mA cm^{-2}).

2.3. Physical characterization: Raman

Raman spectroscopy was performed on an Enwave EZRaman-L series Raman system with excitation light of laser 670 nm wavelength (Enwave Optronics, Inc.) in a dry room (room temperature 25 °C, humidity <2%). The samples were sealed in a cell with a quartz window in a He-filled glove box to reduce any moisture and/or oxygen exposure. In situ Raman spectroscopy was carried out in a custom in situ Raman cell and the electrochemical cell was cycled at a constant current of 3 mA g^{-1} (2.37 mA cm^{-2}).

2.4. Physical characterization: XAS

XAS measurements were performed using a Si (1 1 1) channel cut monochromator in the transmission mode at beamline 18B of the National Synchrotron Light Source (NSLS). The monochromator was detuned to 10% of its original intensity to eliminate the high order harmonics. Energy calibration was carried out using the first inflection point of the spectrum of Mo metal foil as a reference (*i.e.*, Mo K-edge = 19,999 eV). To remove an energy shift problem, the X-ray absorption spectrum for Mo metal foil was measured simultaneously in every measurement as the metal foil was positioned in front of the window of the third ion chamber.

2.5. Electrochemical characterization

Electrochemical properties of SMOF perovskites were tested vs Li metal (Johnson Matthey) by using 2025 type coin cells. The cathodes were introduced by either the use of raw SMOF perovskite powders or the manual mixture of 80 wt% SMOF perovskite powder, 10 wt% carbon black (super P, MMM) and 10 wt% poly(vinylidene fluoride-co-hexafluoropropylene) (PVDF, Kynar 2801, ElfAtochem) binder. Alternatively, free standing electrodes were prepared by casting an acetone based slurry consisting of SMOF, carbon black, poly(vinylidene fluoride-co-hexafluoropropylene) binder and dibutyl phthalate (DBP, Aldrich) plasticizer in the ratio of 39:8:21:32. Once the tape dried, it was placed in 99.8% anhydrous ether (Aldrich) to extract the dibutyl phthalate plasticizer. Disk of about 1 cm^2, typically containing 57% SMOF and 12% SP was punched from these tapes and dried in a He atmosphere for 2 h at 120 °C. The electrodes were separated by a layer of Celgard separator and Whatman GF/D glass fiber separators saturated in the electrolyte consisting of 1 M $LiPF_6$ in ethylene carbonate:dimethyl carbonate (EC:DMC, 1:1 by volume) (Merck). All the cells were assembled under He atmosphere and cycled at constant current 7.58 mA g^{-1} (6 mA cm^{-2}) between 4 and 2 V at 22°C using a MacPile galvanostats (Biologic, Claix, France), unless stated otherwise in the text.

3. Results and discussion

3.1. SMOF perovskite—physical characterization

The evolution of the SMOF perovskites fabricated by high-energy milling the mixtures of AgF and MoO_3 in He atmosphere for 45 min has been investigated by XRD (Fig. 1) and Raman spectroscopy (Fig. 2). As described in the previous paper [7], the SMOF perovskite remained as the significant phase in a wide range of AgF–MoO_3 compositions (x = 1.5–9). Consistent with the idealized stoichiometry, the maximum phase intensity of the perovskite is obtained at x = 3 relative to the minimal quantity of Mo- or Ag-containing minor phases. A small difference throughout a wide composition range is evidenced by the presence of the minor phases consisting of Mo and Ag species varying with Ag:Mo ratio (Fig. 1(b)). When Ag:Mo ratio was less than 3, the minor phase was char-

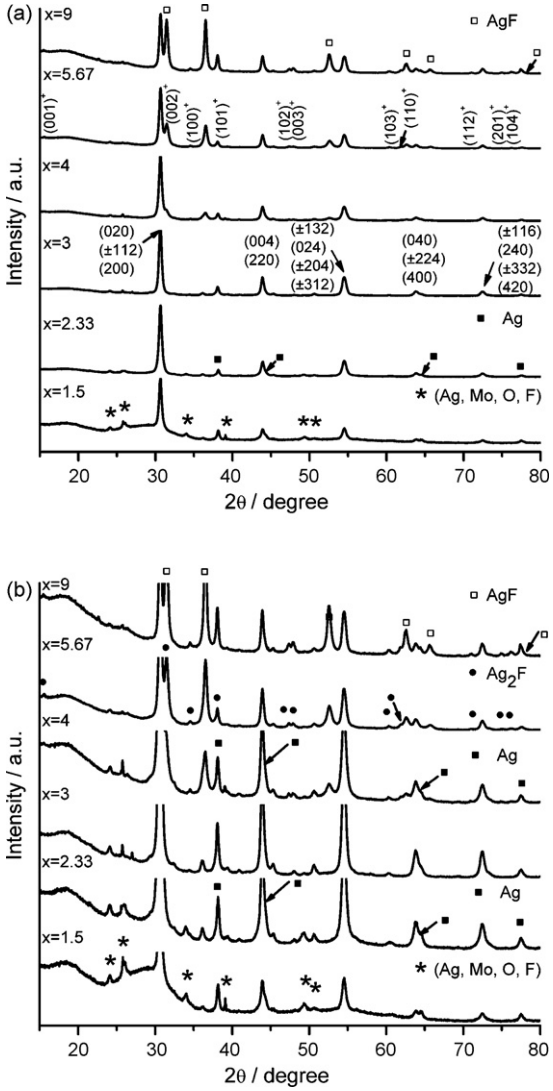

Fig. 1. (a) XRD patterns of high-energy milled AgF and MoO_3 (x = Ag:Mo) for 45 min in He atmosphere. (b) Partial XRD patterns of SMOFs showing the presence of the minor phases: (Ag, Mo, O, F), AgF, Ag and metallic Ag_2F. For SMOF perovskite, only relatively strong Bragg peaks are marked. $(h\,k\,l)^+$ marks the Bragg diffractions related to Ag_2F.

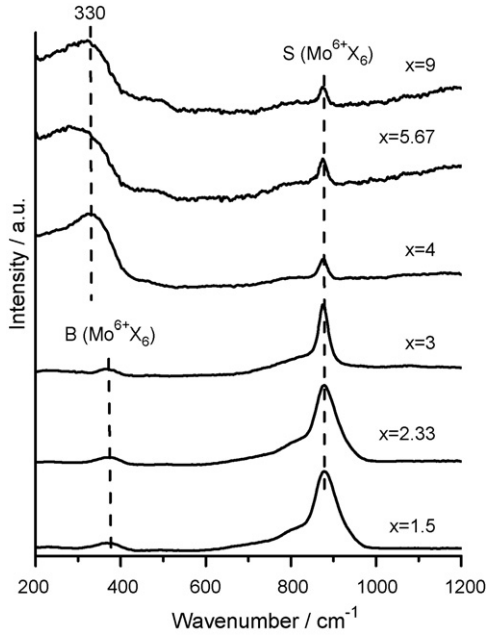

Fig. 2. Raman spectra of high-energy milled AgF and MoO_3 (x = Ag:Mo) for 45 min in He atmosphere.

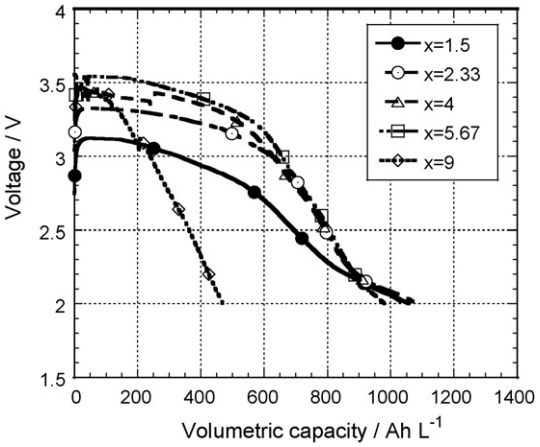

Fig. 3. Voltage vs volumetric capacity for SMOF perovskites fabricated by high-energy milling AgF and MoO_3 (x = Ag:Mo) for 45 min. The cells were cycled at 7.58 mA g^{-1} in 1 M $LiPF_6$ EC:DMC at room temperature.

acterized to be consistent with a yet unknown (Ag, Mo, O and F) phase as crystallization was evident after heat treatment for both samples prepared with AgF and AgF_2. In contrast, high AgF loading (Ag:Mo ≥ 4) resulted in the excess of Ag content in the form of AgF, Ag and Ag_2F with the absence of residual Mo species. It is of particular interest to observe the metallic Ag_2F phase at Ag:Mo ≥ 4 compositions. In these compositions, the relative quantity of these phases is difficult to discern as the Bragg diffractions of Ag_2F overlap with those of Ag and AgF. This is due to its unique anti-CdI_2 structure consisting of hexagonal closed-packed layers of Ag and F atoms. However, Ag_2F phase can be qualitatively characterized by its super structure peak (0 0 1) around 5.672 Å, the intensity of which is about 16% of the most intense peak (1 0 1) around 2.36 Å. Therefore, we could conclude that there is a relatively large amount of Ag_2F phase in these compositions. The presence of Ag_2F is believed to be responsible for the good electrochemical performance found in the sample of x = 5.67. For the composition of x = 9, the relatively poor electrochemical performance was due to the small amount of the SMOF active material and a large amount of AgF residual. The perovskite phase was also affirmed by the observation of the characteristic Raman active bands around 876 and 380 cm^{-1} associated to the stretching (S) and bending (B) vibration mode of MoX_6 octahedron on Fig. 2 as described in more detail in our earlier publication [7]. The apparent shift of the vibration band related to the bending MoX_6 octahedron at $x > 4$ could be due to a distortion of the MoX_6 octahedron or the development of a second phase. It is more likely to result from a second phase as the intensity of the much more intense stretching band around 876 cm^{-1} decreased significantly at $x > 4$. The crystallite size of the as-fabricated SMOF perovskite was calculated to be around 30 nm based on the Scherrer analysis of the most intense (0 2 0) XRD Bragg peak.

3.2. Electrochemical characterization

The as-fabricated samples were introduced in the form of powder and then electrochemically characterized by discharging the SMOFs at 7.58 mA g^{-1} from 4 to 2 V vs Li metal. As opposed to the electrically insulative nature of AgF, SMOF perovskites exhibited a good conductivity, enabling >3 V output voltage and good electrochemical performance of approximately 1000 Ah L^{-1} at moderate rates (Fig. 3) without the use of a carbon matrix in the electrode. Decreasing the cutoff voltage below 2 V would increase the observed capacity as there is clear evidence of an additional cathodic reaction beginning to develop around 2 V. This will be shown later in Fig. 8.

A systematic increase in output voltage from 3.12 to 3.54 V under a current of 7.58 mA g^{-1} parallels the increase in Ag:Mo ratio from x = 1.5 to 5.67. A small decrease to 3.46 V and poor performance was observed for Ag:Mo = 9 (Fig. 3). This systematic variation in the output voltage could be due to the change in the ionicity of chemical bonds in SMOF perovskites as the open-circuit voltage increased from 3.66 to 3.733 V with x ratio before discharge. In contrast, based on the density obtained by He pycnometry, the volumetric capacity of the as-fabricated SMOF perovskites for $x \leq 5.67$ did not vary with the starting materials as all revealed a total volumetric capacity of approximately 1000 Ah L^{-1} during the 1st discharge to 2 V. Except at the stoichiometric extremes, it seems the varied electrochemical performance at various compositions is more likely to be due to the conductivity difference. This is a direct result of the quantity of the dominant active phase (SMOF perovskite) and the secondary-AgF, metallic Ag, Ag_2F phase in the cathode materials as indicated by XRD. This is evident that a significant increase in SMOF content is revealed by XRD from x = 1.5 to 2.33, which is consistent with a large increase in the output voltage. At x = 4, the development of the highly conductive Ag and Ag_2F provides the assistance to the electronic conductivity despite of a small decrease in SMOF content as Ag:Mo ratio is a bit off the idealized stoichiometry. Finally, a relatively large amount of unreacted and insulating AgF phase resulted in the poor electrochemical utilization at x = 9.

3.3. Effect of carbon addition to the electrode

All the data to this point were accomplished without the addition of carbon black to the electrode as the electrochemical activity sans carbon is important for volumetrically intensive applications such as in vivo biomedical. To identify the influence of the electronically conductive carbon, all cathode materials were prepared by manual mixing 80 wt% SMOF perovskite:10 wt% carbon black (SP):10 wt% PVDF (54:23:24 in volume) in He atmosphere. The 1st discharge voltage profiles of manual mixing SMOFs with SP and PVDF as a function of Ag:Mo ratio are shown in Fig. 4. All volumetric capacity numbers are based on the He pycnometry density of SMOF samples. As shown in Fig. 4, of most interest is a

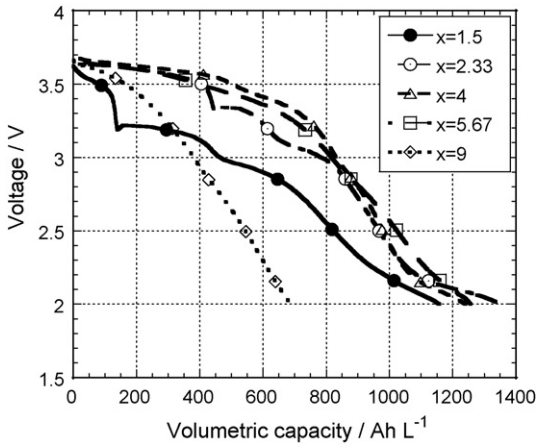

Fig. 4. Voltage vs volumetric capacity plots for Li/$LiPF_6$ EC:DMC/80 SMOF perovskite:10 carbon (SP):10 2801 (wt%) based on the volume and He pycnometry density of SMOF samples. Cells were cycled at 7.58 mA g^{-1} at room temperature. SMOF perovskites were fabricated by high-energy milling AgF and MoO_3 (x = Ag:Mo) for 45 min.

high volumetric capacity of 830 Ah L^{-1} achieved for the sample at Ag:Mo = 4 and 5.67 in the region 4–3 V, which is 87% of theoretical capacity of 954 Ah L^{-1} assuming 3 electrons transfer corresponding to the silver reduction at >3 V for the theoretical composition $Ag_3{}^{1+}Mo^{6+}(O_3F_3)$. This number is about 190% the volumetric capacity of silver vanadium oxide (440 Ah L^{-1}) at >3 V [1], today's state of the art for biomedical applications for high rate and energy density.

Fig. 5 presents the average output voltage and volumetric capacity of SMOFs with and without SP in the high voltage range (>3 V) under a discharge load of 7.58 mA g^{-1}. Overall, the electrochemical performance of SMOFs was improved by SP and an increase in both the average output voltage and the volumetric capacity can be clearly observed to various contents dependent on composition in Fig. 5. It is interesting to note that, unlike raw SMOFs, the average output voltage of SMOFs mixed with SP did not vary with Ag:Mo ratio (Fig. 5(a)). Close examination of Fig. 5(a) revealed a significant increase (ΔV = 0.36 V) in the average voltage of SMOF was observed at Ag:Mo = 1.5 and the enhancement (ΔV) decreased with Ag:Mo ratio and reached to a minimum of 0.02 V at Ag:Mo = 5.67. At very high Ag:Mo ratio (x = 9), a relatively large increase in the voltage difference ΔV = 0.09 V was observed compared to that at x = 5.67. Previously, the variation in the output voltage was assigned to the intrinsic electronic conductivity of SMOFs at various Ag:Mo ratios. As a result, the SMOF sample at x = 5.67 should have the best internal electronic conductivity as it displays a minimal ΔV relative to the carbon assisted sample. This is consistent with the development of metallic Ag_2F phase at this ratio as is clearly indicated by XRD (Fig. 1).

The volumetric capacity is improved by the addition of carbon black due to a decrease in polarization. It should be noted that the prevailing trend of >3 V capacity is established by the relative amount of SMOF perovskite relative to secondary phases and is not a kinetic effect.

3.4. Effect of high-energy milling (HEM) duration

To optimize the electrochemistry of the SMOF perovskites, the mixtures of AgF and MoO_3 with the optimal Ag:Mo = 5.67 composition from above were high-energy milled for the designated times of 15, 30 and 45 min. Only a very small improvement of the electrochemistry of SMOF samples milled for ≥30 min was observed relative to the one milled for 15 min (Fig. 6) regardless of the presence of carbon black. XRD (Fig. 7) revealed that the perovskite phase

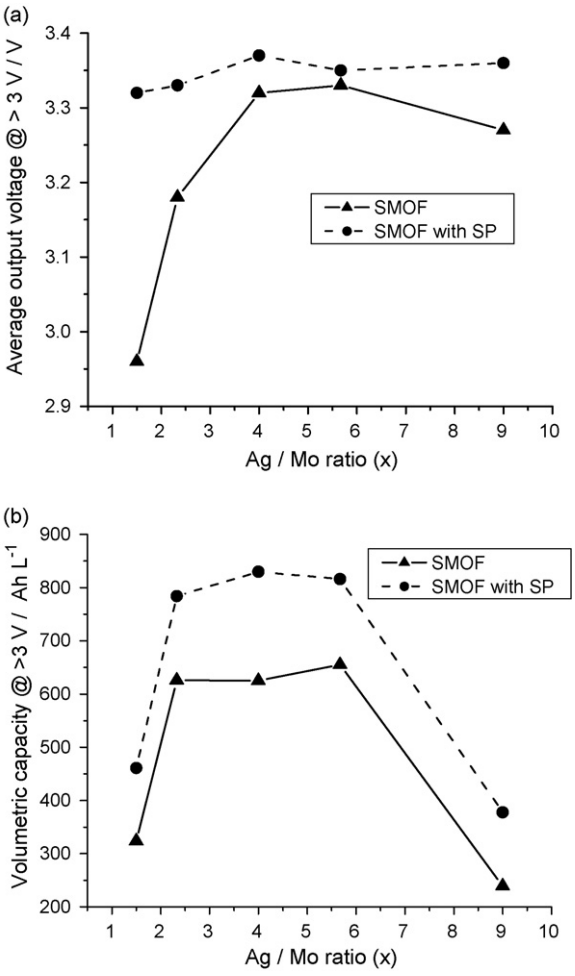

Fig. 5. A comparison of the electrochemical performance of SMOFs mixed with carbon (SP) and SMOFs in terms of (a) average output voltage and (b) volumetric capacity in the high voltage range (>3 V). SMOFs were prepared by high-energy milling AgF and MoO_3 (x = Ag:Mo) in He atmosphere for 45 min and cells were cycled at 7.58 mA g^{-1} at 25 °C.

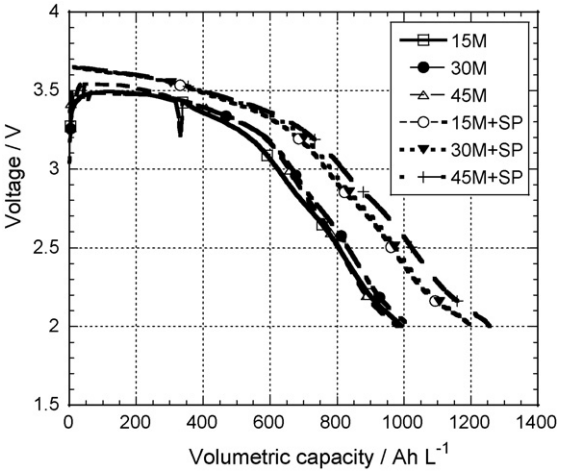

Fig. 6. Voltage profiles of SMOF perovskites as a function of milling time. Labels stand for the high-energy milling time in minutes in He atmosphere. Carbon was introduced by mixing 80 SMOF:10 carbon (SP):10 binder (wt%). Cells were cycled at 7.58 mA g^{-1} in 1 M $LiPF_6$ EC:DMC at 25 °C.

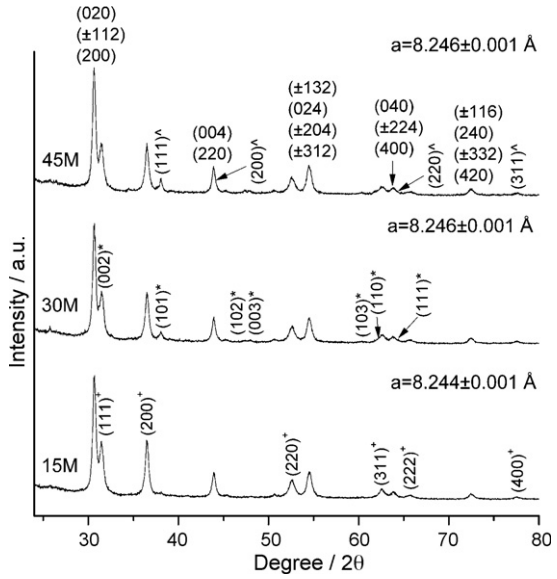

Fig. 7. XRD patterns of high-energy milled AgF and MoO_3 at Ag:Mo = 5.67 for 15, 30 and 45 min in He atmosphere. SMOF perovskite, Ag, AgF and Ag_2F indices are denoted by $(h\,k\,l)$, $(h\,k\,l)$, $(h\,k\,l)^+$ and $(h\,k\,l)^*$ respectively. For SMOF perovskite, only relatively strong Bragg peaks are marked. Lattice parameter in a pseudo-cubic cell of SMOF is given.

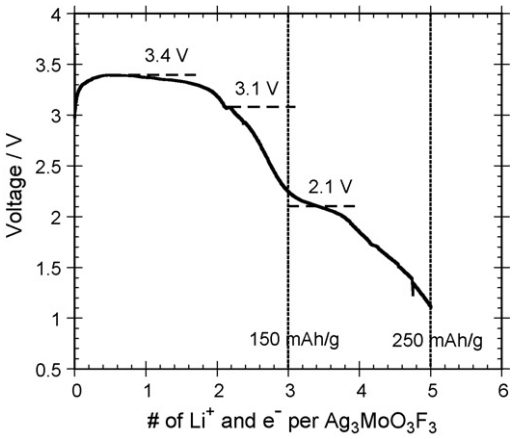

Fig. 8. Voltage profile of a SMOF + Al tape for in situ Raman spectroscopy. SMOF was prepared by high-energy milling AgF and MoO_3 ($x = 2.33$) for 45 min. The cell was cycled at 3 mA g^{-1} in 1 M $LiPF_6$ EC:DMC.

fully developed within 15 min of high-energy milling. The XRD patterns of the powders milled for ≥30 min revealed no evidence of SMOF Bragg peaks broadening or shifting, secondary phase of Ag is present as expected based on the stoichiometry. The lattice parameter in a pseudo-cubic cell of the as-fabricated SMOF given in Fig. 7 shows little difference. This suggests that HEM periods showed little effect on the crystallite size and intrinsic structure of SMOF perovskite.

3.5. Discharge reaction mechanism

Based on the formula $Ag_3MoO_3F_3$, the theoretical capacity of SMOF is calculated to be 153 mAh g^{-1} consistent with a 3 electron silver displacement/reduction in the 3 V region. A 2 electron reduction of Mo^{6+} to Mo^{4+} at a lower voltage results in a total capacity of 255 mAh g^{-1}. The proposed reaction mechanism of SMOF is:

$$Ag_3{}^{1+}Mo^{6+}(O_3F_3) + 5Li^+ + 5e^- \rightarrow 3Ag^0 + Li_5{}^+Mo^{4+}(O_3F_3) \quad (1)$$

Preliminary electrochemical evaluation of SMOF electrode indicated that close to theoretical capacity of 5 inserted Li^+ was achieved with 3 plateaus at 3.6, 3.1 and 2.1 V when discharged to 1.5 V. Our earlier work [7] on an in situ electrochemical study by XRD suggested the insertion of the 3 Li^+ at the 1st plateau (>3 V) was consistent with the displacement, or possible conversion reaction, of SMOF to Ag metal. However, very little useful information

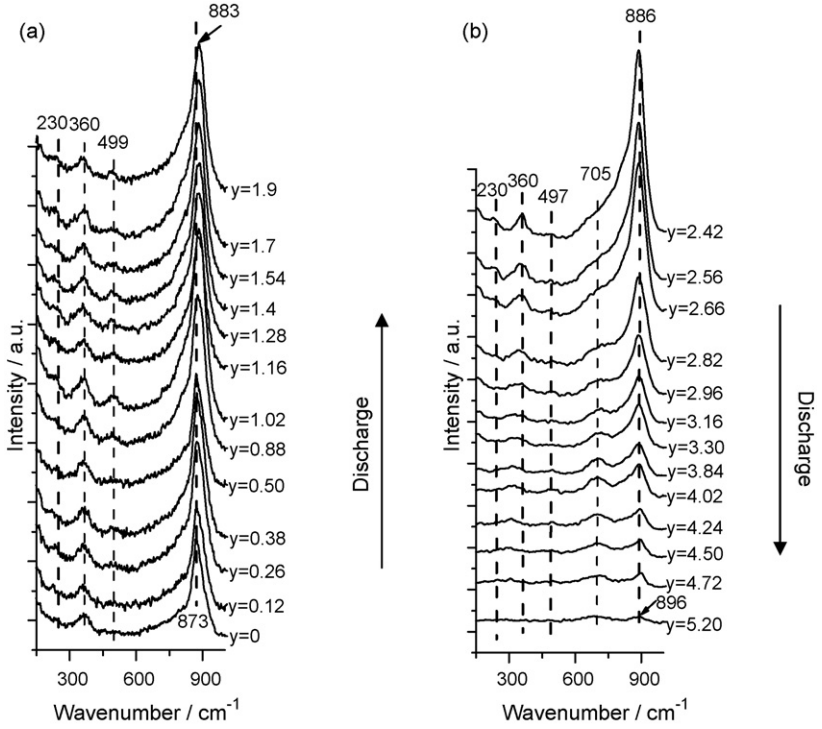

Fig. 9. In situ Raman spectra of a SMOF tape recorded during the 1st discharge. The active material SMOF was fabricated by high-energy milling AgF and MoO_3 ($x = 2.33$) for 45 min. y = # of Li^+/e^- inserted into $Ag_3MoO_3F_3$ formula unit.

could be obtained by in situ XRD as to the nature of the reduction reaction at voltages less than 3 V when the structure was found to transform to an X-ray amorphous like phase. Elucidation of these details with the use of in situ XAS and Raman will be discussed in the next subsections.

3.6. In situ Raman spectroscopy

To reduce the heat generation and improve signal intensity, the electrode for in situ Raman study was fabricated by casting an acetone based slurry containing 60 SMOF:20 Al:20 PVDF (wt%) dispersed in dibutyl phthalate. The SMOF + Al electrode (Fig. 8) revealed 3 plateaus at 3.4, 3.1 and 2.1 V and a specific capacity of 250 mAh g^{-1} when discharged until 1 V. The comparable electrochemical performance to that of SMOF + C electrode [7] assures that it can be used for in situ Raman analysis to understand the underlying electrochemical reaction mechanism.

The in situ Raman spectra of SMOF perovskite during the 1st discharge are shown in Fig. 9. With the insertion of lithium, the Raman spectra of the lithiated phases have the common features to that of the initial SMOF perovskite, consisting of a strong band between 870 and 900 cm^{-1} and several relatively weak bands around 360, 500 and 700 cm^{-1}. At the initial state (3.655 V, $y = 0$), 2 bands are clearly observed at 873 and 368 cm^{-1} (Fig. 9(a)), which were previously assigned to the stretching vibration mode of BX_6 octahedron and the bending vibration mode of BX_6 octahedron respectively.

Fig. 9(a) shows the in situ Raman spectra with the inserted lithium $y = 0 \rightarrow 2$. It can be observed that early in the discharge process ($y = 0.12$), the weak bending band in the low-frequency region red shifted from 366 to 360 cm^{-1} and remained unchanged. In parallel, 2 small new bands at 499 and 230 cm^{-1} developed. From comparison with standards, it was clear that these 2 bands were not due to the vibration of electrolyte (EC and DMC), AlF_3 [8], PVDF binder, $LiPF_6$. Based on a former Raman study [9,10], this is also inconsistent with that of Li_2O. The values of the frequency shift observed in the in situ Raman spectra seem in good agreement with the ones (~240 and 500 cm^{-1}) reported for LiF [11]. The evolution of the LiF bands developed until a maximum was reached at approximately $y = 1.00$.

From $y = 0$ to 0.88, a blue shift of the intense stretching vibration band of BX_6 octahedron from 873 to 878 cm^{-1}, is noted. This band continued to shift to 883 cm^{-1} at $y = 1.02$ and remained unchanged until $y = 1.9$. Therefore, it is considered to be associated to the transition of SMOF perovskite to the in situ X-ray amorphous phase. This slight shift indicates the amorphous phase has the similar local structure to that of SMOF perovskite, suggesting molybdenum octahedra still remained as the major units in the framework of this amorphous phase. Evidence suggests that the perovskite is destabilized by the expelled Ag.

From $y = 1.9$ to 2.42, a blue shift ($883 \rightarrow 886$ cm^{-1}) again developed for the stretching band of BX_6 octahedron and the voltage decreased from 3.24 to 2.9 V. When the output voltage was about 2.9 V ($y = 2.42$), the 886 cm^{-1} band shown a maximal intensity and a new band developed at 705 cm^{-1} (Fig. 9(b)). The 705 cm^{-1} band was not consistent with the vibration of electrolyte (EC, DMC), AlF_3, PVDF binder, $LiPF_6$, Li_2O and LiF. During the insertion of more lithium ($y > 2.42$), the new band at 705 cm^{-1} showed an increase in intensity at the expense of the stretching band of BX_6 octahe-

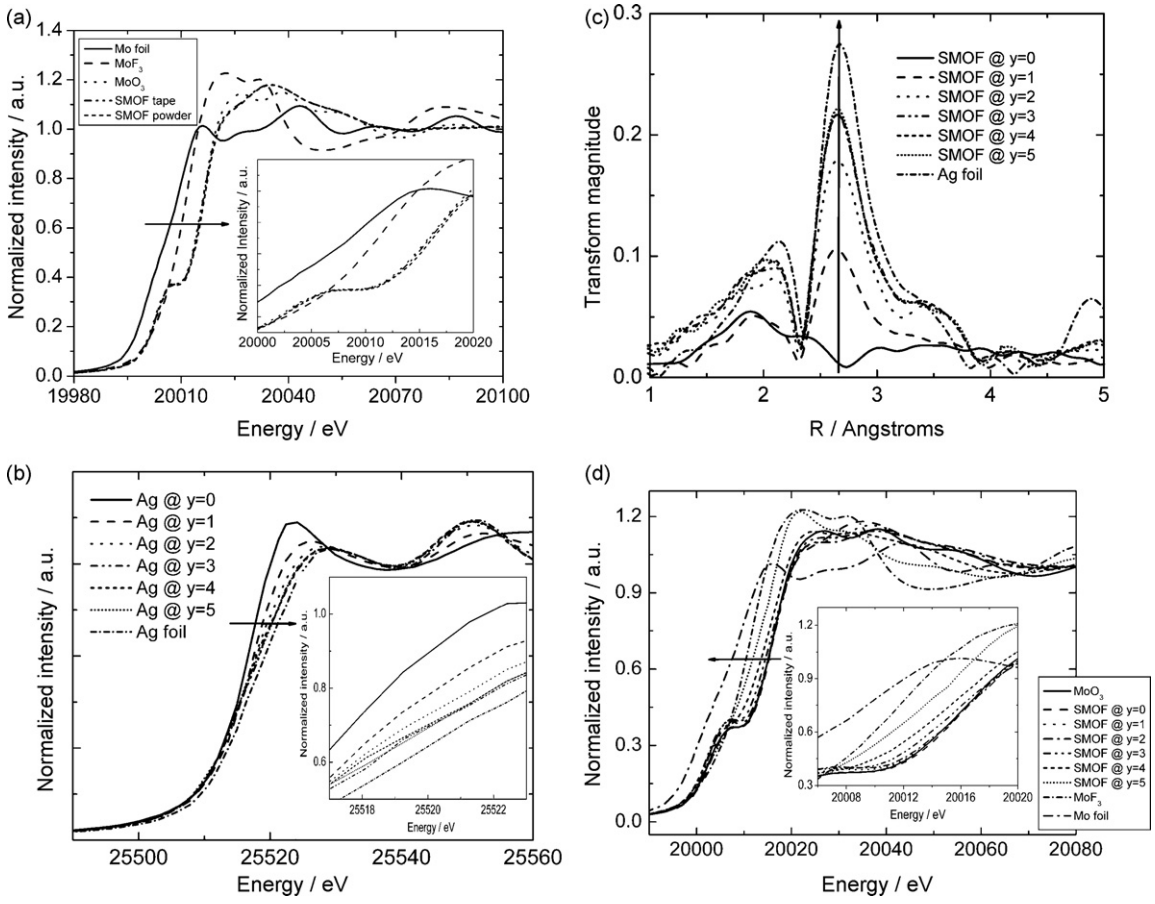

Fig. 10. (a) Mo K-edge XANES spectra comparing Mo in SMOF powder and SMOF tape vs that of Mo^0 foil, $Mo^{3+}F_3$ and $Mo^{6+}O_3$ standards, (b) Ag K-edge XANES spectra during the 1st discharge of the SMOF perovskite, (c) Fourier transforms of Ag K-edge XAS data during the 1st discharge of SMOF and (d) Mo K-edge XANES data during the 1st discharge of SMOF. $y = \#$ of Li^+/e^- inserted into $Ag_3MoO_3F_3$ formula unit.

dra suggesting the origin is linked to the reduction of the Mo^{6+} to a lower oxidation state and the subsequent destruction of the $Mo^{6+}X_6$ octahedron. The stretching vibration band of the remaining BX_6 octahedron remained unchanged until $y = 4$. Further lithium insertion ($y > 4$) resulted in a gradual shift of the very small residual stretching band to 896 cm^{-1}. Consistent with the decrease in voltage and onset of the 2.1 V plateau, the intensity of the Mo-X_6 octahedron stretching and bending bands decreased precipitously suggesting the theoretical reduction of the Mo^{6+} based octahedron induced destruction of the octahedron itself.

3.7. Ex situ X-ray absorption near edge spectroscopy (XANES)

In order to provide a fundamental understanding of the redox reaction on the different lithiation plateaus and support the in situ XRD and Raman results, XAS was employed to monitor the evolution of the electronic and structural modification of Mo of the SMOF perovskite in detail. Fig. 10(a) shows a comparison of the Mo K-edge XANES data for the SMOF perovskite at the initial state along with Mo foil, MoF_3 and MoO_3 reference compounds. A positive energy shift with an increase in formal valency is observed for the Mo K-edge spectra of the various reference compounds. The energy at half-height for both SMOF powder and SMOF + SP tape is consistent with that for $Mo^{6+}O_3$, indicating the valence state of Mo in the SMOF perovskite is 6+. Also no major change in oxidation state was induced by the electrode fabrication process.

The ex situ X-ray absorption near edge structure (XANES) data were collected during the 1st discharge as a function of state of discharge. The spectra (Fig. 10(b)) suggest the continuous change of Ag^+ to metallic Ag^0 during the 1st discharge of the SMOF perovskite. The reduction of Ag^{1+} to Ag^0 metal was almost complete at the theoretical $y = 3$ consistent with the in situ XRD results. Structurally, this conclusion is also supported by the Fourier transform EXAFS data shown in Fig. 10(c) along with that of Ag foil as the reference. The Mo K-edge XANES data during discharge (Fig. 10(d)) show little change in the valence state of Mo^{6+} until $y = 3$. With the further insertion of lithium, a negative energy shift at half-height is observed for the Mo K-edge spectra. At a discharge state of $y = 5$, the energy of Mo K-edge at half-height is clearly observed between that of $Mo^{6+}O_3$ and $Mo^{3+}F_3$. The average valence state of Mo at $y = 5$ is estimated to be 4+.

We have investigated the discharging reaction mechanism of SMOF through in situ XRD, in situ Raman and ex situ XANES techniques. It can be seen in Fig. 11 that from the in situ XRD, the SMOF perovskite peak decreased in intensity as y in Li^+ increased from 0 to 3. By means of in situ XRD and ex situ XANES, the intensity of Ag peak shown a systematic increase up to $y = 3$, and the Mo valence state shown little change until $y = 3$. These results suggest a displacement, or possible conversion reaction of SMOF to Ag metal upon 3 lithium insertion. For $y > 3$, little change of Ag^0 peak was observed, suggesting the end of silver reduction. However, a negative energy shift was observed and the Mo valence state was estimated to be 4+ at $y = 5$. This is in good agreement with the in situ Raman results. A band in the Raman spectra developed at approximately 705 cm^{-1}. This new band showed an increasing intensity relative to the $Mo^{6+}X_6$ octahedron stretching band with more lithium insertion, suggesting its origin is linked to the reduction of the Mo^{6+} to a lower oxidation state.

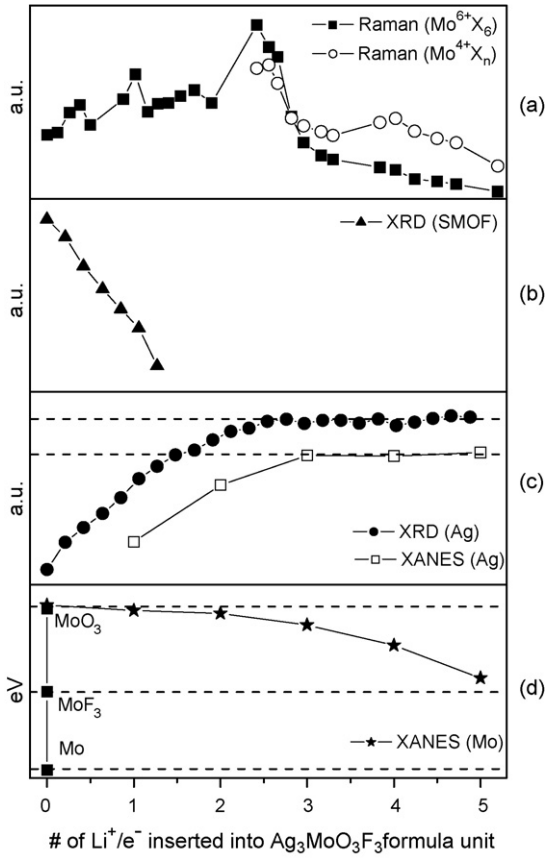

Fig. 11. In situ XRD, in situ Raman and ex situ XANES results: (a) Raman peak intensity of Mo^{6+}- and Mo^{4+}-containing characteristic bands, (b) XRD intensity of SMOF (0 2 0), (c) XRD intensity of Ag^0 (1 1 1) and Fourier transforms of Ag K-edge EXAFS data and (d) Mo K-edge XANES data.

4. Conclusions

The electrochemical properties of an electroactive SMOF perovskite positive electrode were investigated as a function of synthesis condition, stoichiometry and effect of second phases. Without the use of conductive carbon matrix, the best electrochemical performance was observed for SMOF (Ag:Mo = 5.67) with a volumetric capacity of ~1000 Ah L^{-1}. The good conductivity and resulting transport was attributed to the in situ formation of metallic Ag_2F phase during the SMOF fabrication.

With the use of conductive carbon matrix, a high volumetric capacity of 830 Ah L^{-1} was achieved for SMOF ($x = 4$) in the higher voltage region of 4–3 V. This corresponds to 87% of the theoretical capacity (954 Ah L^{-1}) of SMOF assuming 3 Ag^+ reduction at >3 V for the theoretical composition $Ag_3{}^{1+}Mo^{6+}(O_3F_3)$. At 2 V additional capacity attributed to the $Mo^{6+} \rightarrow Mo^{4+}$ reduction lead to an overall volumetric capacity of 1240 Ah L^{-1}.

The underlying reaction mechanism of SMOF during the 1st discharge was investigated by in situ XRD, in situ Raman and ex situ XANES techniques. Both in situ XRD and ex situ XANES clearly revealed a silver displacement or possible conversion reaction at the 1st plateau (>3 V) during the 1st 3 electron transfer. Evidence presented by in situ Raman and ex situ XANES data confirmed the reduction of Mo^{6+} to Mo^{4+} is associated to the 2nd 2 electron transfer.

Acknowledgments

The authors thank Greatbatch Inc. for the financial support of this work. The technical assistance of F. Badway, N. Pereira, I. Plitz, J. Gural and W. Yourey is greatly appreciated.

References

[1] C.F. Holmes, J. Power Sources 97–98 (2001) 739–741.
[2] J. Drews, R. Wolf, G. Fehrmann, R. Staub, J. Power Sources 80 (1999) 107–111.

[3] E.M. Sorensen, H.K. Izumi, J.T. Vaughey, C.L. Stern, K.R. Poeppelmeier, J. Am. Chem. Soc. 127 (2005) 6347–6352.
[4] E.S. Takeuchi, R. Leising, MRS Bull. (U.S.A.) 27 (2002) 624–627.
[5] F. Sauvage, V. Bodenez, H. Vezin, T.A. Albrecht, J.-M. Tarascon, K.P. Poeppelmeier, Inorg, Chem. 47 (2008) 8464–8472.
[6] W. Tong, G.G. Amatucci, ECS Trans. 11 (2008) 19–25.
[7] W. Tong, W.-S. Yoon, N.M. Hagh, G.G. Amatucci, Chem. Mater. 21 (2009) 2139–2148.
[8] S. Kjelstrup Ratkje, E. Rytter, J. Phys. Chem. 78 (1974) 1499–1502.
[9] Y. Ishii, T. Nagasaki, N. Igawa, H. Watanabe, H. Ohno, J. Am. Ceram. Soc. 74 (1991) 2324–2326.
[10] T. Osaka, I. Shindo, Solid State Commun. 51 (1984) 421–424.
[11] G.N. Papatheodorou, V. Dracopoulos, Chem. Phys. Lett. 241 (1995) 345–350.